

## Washington University School of Medicine Digital Commons@Becker

---

### Open Access Publications

---

2007

# Diffusion tensor imaging predicts hyperacute spinal cord injury severity

David N. Loy

*Washington University School of Medicine*

Joong Hee Kim

*Washington University School of Medicine*

Mingqiang Xie

*Washington University School of Medicine*

Robert E. Schmidt

*Washington University School of Medicine*

Kathryn Trinkaus

*Washington University School of Medicine*

*See next page for additional authors*

Follow this and additional works at: [http://digitalcommons.wustl.edu/open\\_access\\_pubs](http://digitalcommons.wustl.edu/open_access_pubs)

---

### Recommended Citation

Loy, David N.; Kim, Joong Hee; Xie, Mingqiang; Schmidt, Robert E.; Trinkaus, Kathryn; and Song, Sheng-Kwei, "Diffusion tensor imaging predicts hyperacute spinal cord injury severity." *Journal of Neurotrauma*.24,6. 979-990. (2007).  
[http://digitalcommons.wustl.edu/open\\_access\\_pubs/4742](http://digitalcommons.wustl.edu/open_access_pubs/4742)

This Open Access Publication is brought to you for free and open access by Digital Commons@Becker. It has been accepted for inclusion in Open Access Publications by an authorized administrator of Digital Commons@Becker. For more information, please contact [engeszer@wustl.edu](mailto:engeszer@wustl.edu).

---

**Authors**

David N. Loy, Joong Hee Kim, Mingqiang Xie, Robert E. Schmidt, Kathryn Trinkaus, and Sheng-Kwei Song

## Diffusion Tensor Imaging Predicts Hyperacute Spinal Cord Injury Severity

DAVID N. LOY,<sup>1,\*</sup> JOONG HEE KIM,<sup>1,\*</sup> MINGQIANG XIE,<sup>1</sup> ROBERT E. SCHMIDT,<sup>2</sup>  
KATHRYN TRINKAUS,<sup>3</sup> and SHENG-KWEI SONG<sup>1</sup>

### ABSTRACT

Experimental strategies that focus on ventral white matter (VWM) preservation during the hyperacute phase hold great potential for our improved understanding of functional recovery following traumatic spinal cord injury (SCI). Critical comparisons of human SCI to rapidly accumulating data derived from rodent models are limited by a basic lack of *in vivo* measures of subclinical pathophysiological changes and white matter damage in the spinal cord. Spinal cord edema and intraparenchymal hemorrhage demonstrated with routine MR sequences have limited value for predicting functional outcomes in SCI animal models and in human patients. We recently demonstrated that *in vivo* derived diffusion tensor imaging (DTI) parameters are sensitive and specific biomarkers for spinal cord white matter damage. In this study, non-invasive *in vivo* DTI was utilized to evaluate the white matter of C57BL/6 mice 3 h after mild (0.3 mm), moderate (0.6 mm), or severe (0.9 mm) contusive SCI. In the hyperacute phase, relative anisotropy maps provided excellent gray-white matter contrast in all degrees of injury. *In vivo* DTI-derived measurements of axial diffusion differentiated between mild, moderate, and severe contusive SCI with good histological correlation. Cross-sectional regional measurements of white matter injury severity between dorsal columns and VWM varied with increasing cord displacement in a pattern consistent with spinal cord viscoelastic properties.

**Key words:** anisotropy; axial diffusion; diffusion tensor imaging; hyperacute; ischemia; magnetic resonance; mouse; radial diffusion; spinal cord injury

### INTRODUCTION

**D**ESPITE MANY RECENTLY REPORTED ADVANCEMENTS in the field of traumatic spinal cord injury (SCI), measures of ongoing pathophysiological processes in the injured spinal cord remain elusive during the critical hyperacute phase (0–6 h after SCI). Standard clinical

magnetic resonance imaging (MRI) sequences effectively identify spinal cord compression, edema, and hemorrhage. Large intraparenchymal hemorrhages are a well-known predictor of poor outcome following SCI when present (Boldin et al., 2006). However, the presence of spinal cord T2 hyperintensity does not predict functional outcomes as large regions of increased T2 signal may be

---

Departments of <sup>1</sup>Radiology, <sup>2</sup>Pathology, and <sup>3</sup>Biostatistics, Washington University, Saint Louis, Missouri.

\*These authors contributed equally to this article.

associated with an incomplete neurologic injury while a smaller region may be present in patients with complete paralysis below the injury level (Shepard and Bracken, 1999). Current MRI sequences do not provide information about the integrity of critical white matter long tracts responsible for observed functional deficits after SCI.

Diffusion tensor imaging (DTI) measures water diffusion anisotropy in live tissues. Quantitative DTI parameters such as apparent diffusion coefficient (ADC), relative anisotropy (RA), fractional anisotropy (FA), and trace of diffusion tensor (Tr) have been utilized extensively to study brain development and evolving pathologic changes in a number of central nervous system (CNS) diseases, most notably stroke, where ADC is routinely employed clinically for early diagnosis of ischemia (Le Bihan et al., 2001; Basser and Jones, 2002; Sotak, 2002; Sundgren et al., 2004). Application of DTI to experimental rodent models of SCI *in vivo* has been limited by low signal-to-noise ratios (SNR) of diffusion measurements (Schwartz and Hackney, 2003). However, initial studies following ischemic photochemical SCI in mice proved that contrast between normal and injured white matter could be demonstrated with DTI (Bonny et al., 2004). Deo et al. (2006) subsequently suggested that changes in rostral white matter axial diffusion ( $\lambda_{\parallel}$ ), diffusion parallel to the longitudinal axis of the spinal cord, after SCI in rats also correlated with overground locomotor scores in the chronic phase. Recently, we reported directional diffusivities in the spinal cords of experimental autoimmune encephalomyelitis (EAE) mice and within the optic nerve following retinal ischemia. Decreases in  $\lambda_{\parallel}$  and increases in radial diffusion orthogonal to the longitudinal axis of the spinal cord ( $\lambda_{\perp}$ ) proved sensitive and specific biomarkers of axonal and myelin damage, respectively, in mice (Song et al., 2003; Kim et al., 2006). These studies suggest that DTI may be particularly well-suited for measurements of damaged myelinated long tracts in the spinal cord following traumatic injury. Present studies were undertaken to demonstrate the efficacy of DTI-derived parameters at predicting the degree of white matter damage following graded contusive SCI in the clinically relevant hyperacute phase.

## METHODS

### *Spinal Cord Injury*

All surgical interventions and both pre- and post-surgical care were provided in accordance with the Public Health Service Policy on Humane Care and Use of Laboratory Animals, *Guide for the Care and Use of Laboratory Animals* (Institute of Laboratory Animal Resources, National Research Council, 1996), and with the

approval of the Washington University Animal Studies Committee.

Twenty 12-week-old female C57BL/6 mice weighing 19–22 g (Harlan–Sprague Dawley, Inc., Indianapolis, IN) were anesthetized with a mixture of ketamine (80 mg/kg) and xylazine (10 mg/kg) intraperitoneally. After dorsal laminectomy at the T12 vertebral level, mice received 0.3 mm ( $n = 5$ ), 0.6 mm ( $n = 5$ ), or 0.9 mm ( $n = 5$ ) contusive SCIs utilizing a modified OSU impactor (1.7 mm round impactor tip, 0.9 mm impact distance, 0.15 m/sec impact speed). Five mice received sham laminectomy only. The surgical site was closed in layers with 4-0 Vicryl and nylon sutures. Injection of lactated ringers was administered subcutaneously.

### *Animal Preparation for In Vivo Diffusion Tensor Imaging*

Following laminectomy and SCI, mice were placed into a nose cone, and the vertebral column was immobilized with a custom-made nylon mounting device described previously (Kim et al., 2006). An isoflurane and oxygen mixture (0.7–1.5%) was used for anesthesia maintenance inside the magnetic resonance (MR) scanner. Core body temperatures were maintained at  $37.0 \pm 0.5^{\circ}\text{C}$  with a circulating warm water pad. The respiratory exhaust line was connected to a pressure transducer to synchronize DTI data collection with the animal's respiratory rate. Details of the respiratory gating technique have been reported previously (Garbow, 2004).

An inductively coupled surface coil covering T11–T13 vertebral segments (15 mm  $\times$  8 mm) was used as the radio frequency (RF) receiver. A 9-cm i.d. Helmholtz coil was employed as the RF transmitter. The preparation was placed in an Oxford Instruments 200/330 magnet (4.7 T, 33-cm clear bore) equipped with a 15-cm inner diameter, actively shielded Oxford gradient coil (18 G/cm, 200- $\mu\text{sec}$  rise time). The magnet, gradient coil, and Techtron gradient power supply were interfaced with a Varian UNITY-INOVA console controlled by a Sun Microsystems Ultra-60 Sparc workstation.

### *In vivo Diffusion Tensor Imaging*

A conventional spin-echo imaging sequence was modified by adding Stejskal-Tanner diffusion-weighting gradients (Stejskal, 1965). The spin echo time (TE) = 38 msec, time between application of gradient pulses ( $\Delta$ ) = 20 msec, and diffusion gradient on time ( $\delta$ ) = 7 msec, were fixed throughout experiment. The repetition time (TR;  $\sim 1.2$  sec) was varied according to the period of respiratory cycle ( $\sim 270$  msec). Three different image slices

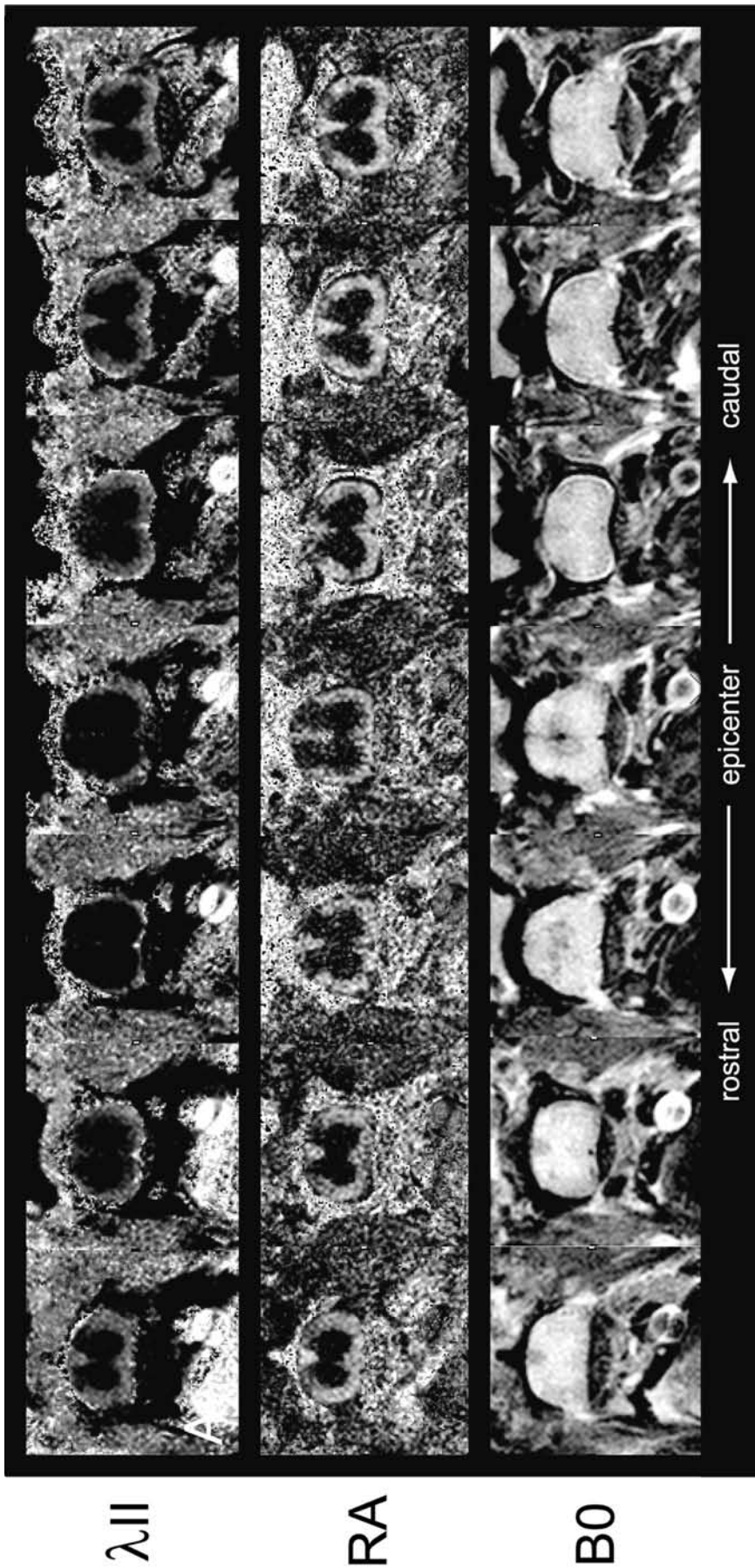


**FIG. 1.** Representative *in vivo* diffusion tensor imaging (DTI) of hyperacute spinal cord injury (SCI; 0.9 mm displacement) spanning T11–T13. First row images show marked reductions in white matter  $\lambda_{||}$  at the impact epicenter indicating severe white matter injury. In the second row, relative anisotropy (RA) maps provide contrast necessary to define gray-white matter borders after SCI. Third row images are displayed without diffusion weighting (B0) (4.7 T, TE = 38 msec, TR varied with respiratory rate  $\sim$ 1.2 sec,  $\Delta$  = 20 msec,  $\delta$  = 7 msec, slice thickness = 0.75 mm, in-plane resolution =  $75 \mu\text{m}^2$ ).

were collected during every breath. Images were obtained with diffusion sensitizing gradients applied in six orientations:  $(G_x, G_y, G_z) = (1, 1, 0), (1, 0, 1), (0, 1, 1), (-1, 1, 0), (0, -1, 1),$  and  $(1, 0, -1)$ . Two diffusion-sensitizing  $b$  values, 0 and  $0.785 \text{ msec}/\mu\text{m}^2$ , were used. The chosen  $b$  value,  $0.785 \text{ msec}/\mu\text{m}^2$ , is similar to previous DTI measurements in animal models and represented optimal experimental conditions within the gradient power limits of our system (Madi et al., 2005; Hassan et al., 2006). Higher  $b$  values obtained by increasing  $\Delta$  would have limited diffusion measurements because of resultant decreases in SNR. Eight scans were averaged per  $k$ -space line with field of view  $1 \times 1 \text{ cm}^2$  and data matrix  $128 \times 128$  (zero filled to  $256 \times 256$ ).

The localization of vertebral segments was achieved by referencing the ilium on the coronal scout image. Nine transverse images (slice thickness, 0.75 mm) were collected covering vertebral segments T11–T13. Average scan time was 2.5 h.

### Data Analysis

The eigenvalues ( $\lambda_1, \lambda_2,$  and  $\lambda_3$ ) and eigenvectors of the diffusion tensor, the trace of the diffusion tensor (trace), axial diffusivity ( $\lambda_{\parallel}$ ), radial diffusivity ( $\lambda_{\perp}$ ), and RA were derived from diffusion-weighted images using software written in Matlab (MathWorks, Natick, MA) as described previously (Sun et al., 2003):

$$\text{Trace} = \lambda_1 + \lambda_2 + \lambda_3 \quad (1)$$

$$\lambda_{\parallel} = \lambda_1 \quad (2)$$

$$\lambda_{\perp} = (\lambda_2 + \lambda_3)/2 \quad (3)$$

$$\text{RA} = \frac{\sqrt{(\lambda_1 - \langle D \rangle)^2 + (\lambda_2 - \langle D \rangle)^2 + (\lambda_3 - \langle D \rangle)^2}}{\sqrt{3} \langle D \rangle} \quad (4)$$

In sham-operated control animals, the manual segmentation of white matter for region of interest (ROI) analysis was performed based on DTI parameters maps. Mean RA values of normal gray matter were used as the

reference to assure the objectivity of ROI analysis on residual dorsal columns (DC) and ventral white matter (VWM) after contusion injury. The delineated DC and VWM ROIs were applied to the non-diffusion-weighted images ( $b = 0 \text{ msec}/\mu\text{m}^2$ ) for SNR calculations. SNR was defined as the quotient of the mean signal intensity and standard deviation (SD) of the background noise multiplied by 0.66 in consideration of Rayleigh statistics (Edelstein et al., 1984).

### Tissue Preparation and Histological Analysis

At the conclusion of *in vivo* DTI examinations, all mice were perfusion fixed through the left ventricle under deep anesthesia with 50 mL of 0.1 M phosphate-buffered saline (PBS) (pH 7.4) followed by 200 mL of 0.1 M PBS containing 4% paraformaldehyde (pH 7.4). Following fixation, the spine was harvested, left in the fixative for 24 h, decalcified, embedded in paraffin, and then sectioned on a sliding microtome ( $3 \mu\text{m}$ ). A 2-mm segment of spinal cord centered at the contusion epicenter was cut with the decalcified vertebral column intact. For examination of myelin integrity, luxol fast blue (LFB) staining was conducted. After deparaffinization, rehydration, and immersion in LFB solution ( $56^\circ\text{C}$ ), excess stain was rinsed off and differentiation was performed with lithium carbonate solution and ethyl alcohol. After completion of differentiation, tissue was mounted for microscopic inspection. Silver staining (modified Bielschowsky method) was performed for microscopic examination of axons. Sections immediately adjacent to those utilized for LFB staining were used. Samples were placed in sodium thiosulfate followed by incubation with  $\text{AgNO}_3$  ( $4^\circ\text{C}$ ). Development was quenched with 1% acetic acid.

For immunohistochemistry, randomly selected sections from each spinal cord sample were deparaffinized and rehydrated. Antigen retrieval was employed. Briefly, sections were placed in 1mM EDTA and maintained at  $95\text{--}100^\circ\text{C}$  in a water bath. Slides were rinsed in 0.01M PBS for 10 min and incubated with 0.01M PBS containing a 2% blocking solution (Invitrogen, Carlsbad, CA) for 1 h. Sections were then incubated with one or more

**FIG. 2.** Axial diffusion ( $\lambda_{\parallel}$ ) accurately predicts hyperacute spinal cord injury (SCI) severity. Representative *in vivo* spinal cord relative anisotropy (RA; **A**) and  $\lambda_{\parallel}$  (**B**) maps are displayed 3 h after sham laminectomy (control), mild (0.3 mm displacement), moderate (0.6 mm), or severe (0.9 mm) SCI (impact velocity = 0.15 m/sec). Tracing gray-white boundaries on RA maps is beneficial for reducing quantification errors after SCI (**A**). RA maps alone are ineffective discriminating measures of injury severity (**L,M**).  $\lambda_{\parallel}$  is a sensitive and specific quantitative measure of white matter damage in the hyperacute phase (**B,N,O**). Arrowheads (row B, 0.6 mm) demonstrate a slightly asymmetric margin of axonal injury in the dorsal columns (DC) and ventral white matter (VWM). Representative modified Bielschowsky silver-stained transverse sections of DC (**C,E,G,I**) and VWM (**D,F,H,J**) show a typical combination of swollen and compacted axons associated with ovoid lucencies in the white matter during the hyperacute phase (20 $\times$  magnification, inset 40 $\times$ , error bars = 20  $\mu\text{m}$ ). These changes appear more prominent with increasing SCI severity, consistent with DTI-predicted white matter injury (**K**), representative low-magnification (4 $\times$ ) images of silver stained spinal cords and severe (0.9 mm) SCI. \* $p < 0.05$ , \*\* $p < 0.01$ , \*\*\* $p < 0.001$ .

DTI OF HYPERACUTE SPINAL CORD INJURY

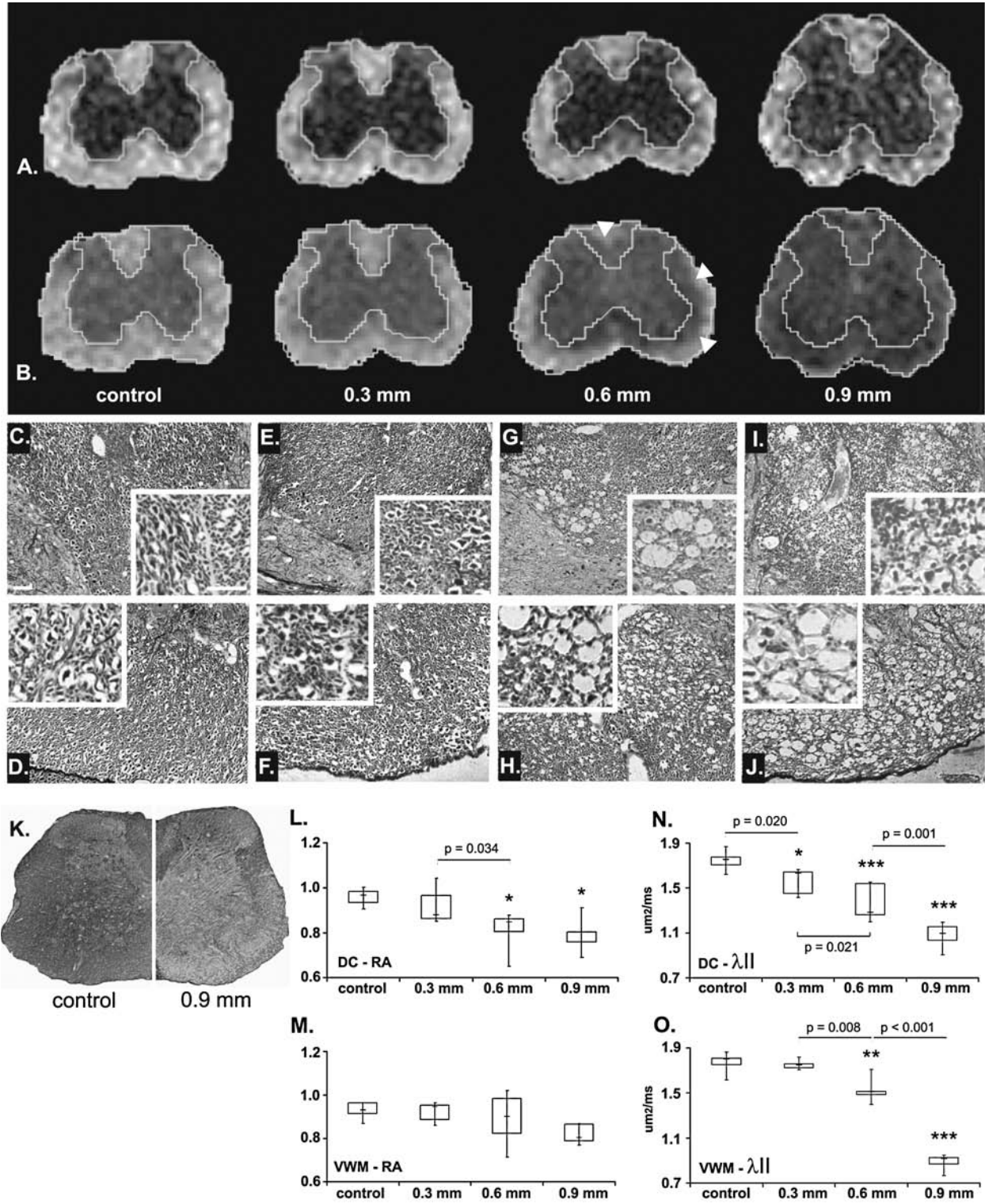


FIG. 2.

of the following primary antibodies: polyclonal anti-myelin basic protein (1:1000; Sigma Chemical Co., St. Louis, MO), monoclonal anti-SMI31 (1:5000) and anti-SMI32 (1:5000) or SMI38 (1:5000), to label phosphorylated and dephosphorylated neurofilaments, respectively (Sternberger Monoclonals, Inc., Lutherville, MD). All incubations were at 4°C overnight. Sections were washed with 0.01M PBS three times. Fluorescein isothiocyanate (FITC)-conjugated Fab' fragments (goat anti-mouse or rabbit, 1:300; Jackson ImmunoResearch Laboratories, Inc., West Grove, PA) in 0.01M PBS were applied to sections and allowed to incubate at room temperature for 1 h. After washing with PBS, sections were cover-slipped using the Vectashield Mounting Medium with DAPI (Vector Laboratories, Burlingame, CA). All images were captured within 1 week following completion of immunohistochemistry.

### Statistical Analysis

Linear regression models were used to describe differences in DTI parameters (relative anisotropy, axial and radial diffusivity) associated with impact depth (0.0, 0.3, 0.6, or 0.9 mm) and location of injury (DC or VWM). The DTI parameters are dependent variables in these models; one model was created for each parameter. The independent variables (predictors) were impact depth, location of injury and the interaction of impact depth and location. The interaction term tests whether the effect of impact depth on each DTI parameter differs in dorsal and ventral white matter. Each mouse contributed two observations to each model, as each mouse received one injury and DTI parameters were measured at two locations in each mouse. A clustered model was used to take into account the correlation between observations made in dorsal and ventral white matter within each mouse. Hypotheses were tested using contrasts, which are linear combinations of independent variables in each model. In

addition to testing the effects of impact depth, impact location and their interaction, 12 hypothesis tests were carried out. Each test compared the effect on one DTI parameter of injuries at one location but of different depths. For example, RA in the dorsal white matter of uninjured mice versus mice with a 0.3-mm injury, or radial diffusion in the ventral white matter of mice receiving injuries of 0.3 versus 0.9 mm. The probability of a falsely positive result among 12 tests is reasonably high, so a Hochberg step-up procedure was used to correct the  $p$ -values for multiple tests. All models were created in SAS v9.1.3 using proc mixed and proc multtest.

## RESULTS

### Spinal Cord Diffusion Tensor Imaging

The transverse diffusion image slices of mouse spinal cords were prescribed on a coronal anatomic image. After hyperacute SCI, excellent contrast between gray and white matter was observed in RA maps (Figs. 1 and 2A). Cerebrospinal fluid (CSF) appears dark on RA maps and bright on axial and radial diffusivity maps indicating low anisotropy. Group averaged DTI parameters and the SNR of VWM were obtained using a ROI analysis. ROIs within DC and VWM were traced on RA maps post-injury. Quantitatively, RA was an ineffective discriminating measure of injury severity (Fig. 2A,L,M). Within the DCs, no significant RA differences were observed between normal and mild injuries or between moderate and severely injured groups. Quantitative measurements collocated the four experimental groups into sham or mild SCI, and moderate-severe SCI ( $p = 0.034$ ). No significant RA changes were demonstrated between experimental groups within VWM ( $p = 0.21$ , control vs. 0.9 mm; Fig. 2M).

Axial diffusion measurements accurately predicted hyperacute SCI severity (Fig. 2B,N,O). DC axial diffusion

---

**FIG. 3.** Regional comparisons of  $\lambda_{||}$  and hyperacute axonal injury. Representative SMI31 or SMI32-immunostained transverse spinal cord sections after laminectomy only (A–D,Q) and after 0.3 mm (E–H), 0.6 mm (I–L), or 0.9 mm (M–P,R) spinal cord injury (SCI) are presented with regional quantitative  $\lambda_{||}$  comparisons (S). No qualitative changes in axonal SMI31 immunostaining were observed between injury groups during the hyperacute phase. Consistent with  $\lambda_{||}$  measurements (S,  $df = 1,32$ ;  $F = 7.82$ ;  $p = 0.009$  for dorsal column vs ventral white matter), 0.3 mm of dorsal displacement results in qualitative increases in white matter SMI32-immunostaining indicative of axonal injury primarily in the dorsal columns (compare B–D to F–H). SMI32-positive axonal staining confirms  $\lambda_{||}$ -predicted differences in DC and VWM damage after 0.6 mm injuries ( $df = 1,32$ ;  $F = 5.41$ ;  $p = 0.027$ , compare F–H to J–L).  $\lambda_{||}$  measurements after severe SCI (0.9 mm) suggest more severe damage within VWM compared to DC ( $df = 1,32$ ;  $F = 8.12$ ;  $p = 0.008$ ; N–P). This apparent reversal between the degree of DC and VWM damage may result from the distribution of force tensors within the spinal cord during larger displacements. Representative low-magnification (4×) SMI32-immunostained sections are shown in Q and R, respectively. Sections in columns 1 and 2 represent the same animal within each injury group. Columns 2–4 display sections from different animals within each group. All error bars = 20  $\mu\text{m}$ . \* $p < 0.05$ , \*\* $p < 0.01$ .

DTI OF HYPERACUTE SPINAL CORD INJURY

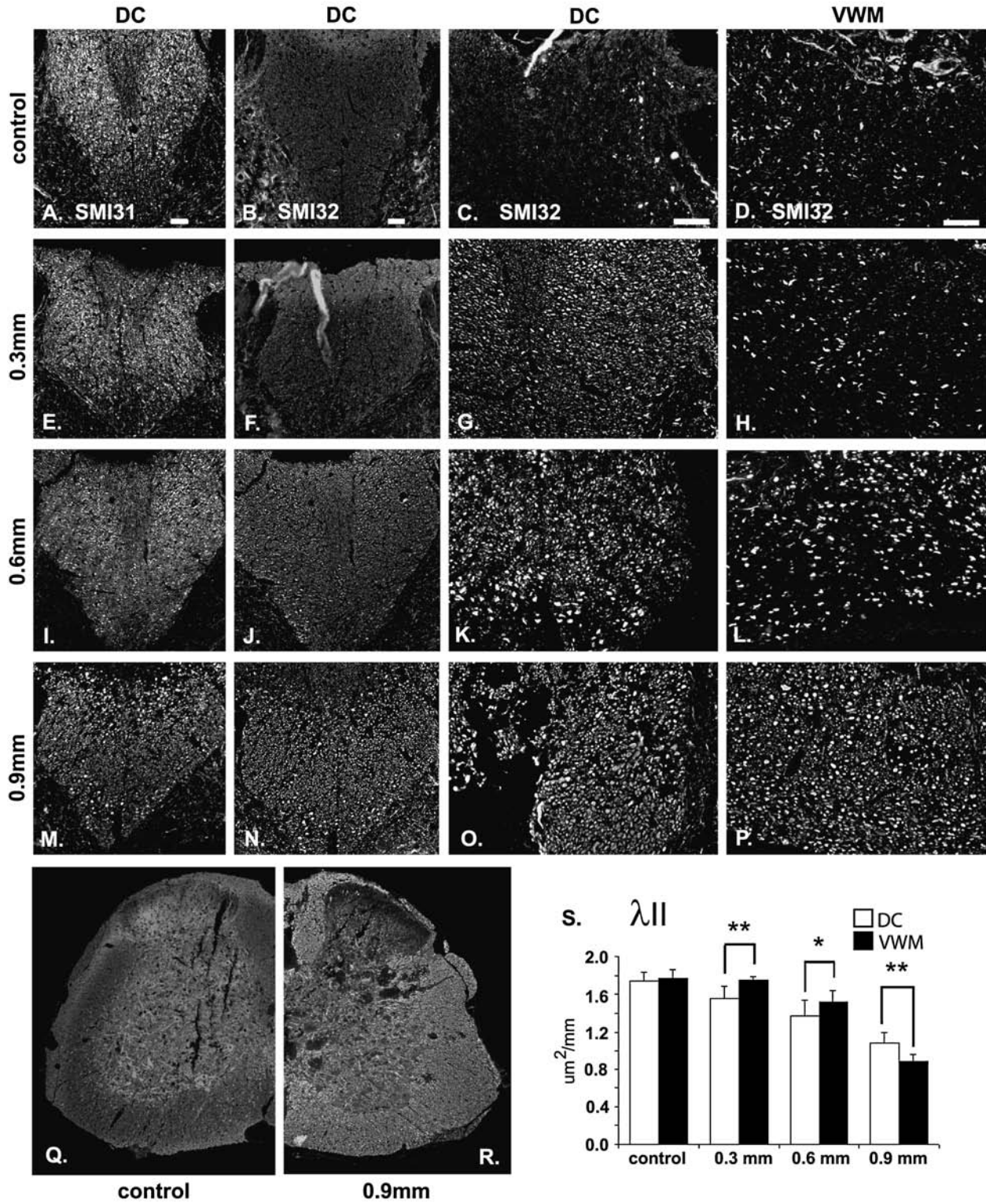


FIG. 3.

measured  $1.75 \pm 0.09$ ,  $1.56 \pm 0.12$ ,  $1.37 \pm 0.17$ , and  $1.08 \pm 0.11 \mu\text{m}^2/\text{msec}$  in sham, and 0.3, 0.6, and 0.9 mm SCI, respectively. Statistically significant differences were demonstrable between all injury groups (Fig. 2N). In VWM, 0.6 mm and 0.9 mm injuries measured  $1.52 \pm 0.11$  and  $0.89 \pm 0.07 \mu\text{m}^2/\text{msec}$ , respectively (0.6 mm,  $p = 0.005$ ; 0.9 mm,  $p < 0.0001$  compared to control). The 0.6 and 0.9 mm injuries were easily distinguished, both visually and quantitatively ( $p < 0.0001$ ). No difference was detected between sham and 0.3 mm injuries within VWM. This result was expected because 0.3 mm of displacement produces an injury localized primarily to the DC. Interestingly, severe injuries (0.9 mm) resulted in lower axial diffusion measurements in VWM when compared to DC (Fig. 3S). Tr images followed similar trends, weighted by marked changes in the longitudinal  $\lambda_1$  eigenvalue (Fig. 4).

Radial diffusion decreased significantly only within VWM ( $p = 0.032$ ) and only within the most severe regions of axonal damage as evidenced by histological staining (compare Figs. 2 and 4). No significant change in radial diffusion was demonstrated between hyperacute injury groups within the DC.

Axial diffusivity in normal spinal cords was higher in white matter than that measured in the gray matter (data not shown). In contrast, gray matter radial diffusivity was higher than that in the white matter (Kim et al., 2006). VWM axial diffusivity was approximately sixfold that of radial diffusivity. Consistent with previous reports from our laboratory, the RA ratio of white matter to gray matter was approximately three (Kim et al., 2006).

### Histology of Spinal Cord Injury

Standard silver, LFB, and immunohistochemical stains were performed to validate MR measurements of white matter injury. *In vivo* DTI findings were evaluated by matching histological sections from the epicenter approximately 3 h after injury. Silver and immunohistochemical stains confirm DTI-predicted white matter injury that appeared progressively worsened with each increase in SCI severity. Axonal swelling and periaxonal ovoid lucencies indicative of cytotoxic edema and acute

white matter necrosis were observed in DC and VWM following 0.6 and 0.9 mm SCIs (Fig. 2C–J). Antibodies directed at nonphosphorylated epitopes of neurofilament H (SMI 32 and SMI38) also showed axonal injury within the DC of 0.3 mm injuries (Fig. 3B,C,F,G). No histological evidence for axonal injury is present in the VWM of animals following 0.3 mm injuries. This result was expected because 0.3 mm injuries produce injury primarily in the DC. Increases in SMI 32 staining were also apparent in both DC and VWM after 0.6 and 0.9 mm injuries (Fig. 3J–L,N–P). The observed radial pattern of white matter injury with increasing injury severity is consistent with multiple reports describing standardized dorsal contusive injuries. Consistent with reports by Zhang et al., no qualitative reduction in phosphorylated neurofilament staining (SMI31) was observed within intact axons during the hyperacute phase (Zhang et al., 2000) (Fig. 3).

Within the epicenter, LFB stains demonstrated essentially normal appearing DC and VWM myelin following mild and moderate injuries consistent with quantitative  $\lambda$  (Fig. 4I,L,M). Relative decreases in LFB staining were seen only after 0.9 mm SCI (Fig. 4I, lower right). However, antibodies directed against MBP demonstrated no evidence for demyelination in the hyperacute phase (Fig. 4J,K). Rather, apparent decreases in LFB staining appeared to result from the aforementioned changes of white matter necrosis and cytotoxic edema. Multiple intraparenchymal hemorrhages were seen arising predominantly within gray matter after 0.9 mm SCI. Foci of blood products were also observed in the white matter, most notably within the DC.

## DISCUSSION

These studies demonstrate for the first time that non-invasive assessments of spinal cord white matter injury severity can be obtained in mice during the clinically relevant hyperacute phase (0–6 h) after SCI using MRI. *In vivo* DTI-derived axial diffusivity differentiated mild, moderate, and severe contusive SCI at 3 h with good his-

---

**FIG. 4.** Hyperacute radial diffusion ( $\lambda_{\perp}$ ) and trace (Tr) measurements. Transverse  $\lambda_{\perp}$  images (A–D) demonstrate significant decreases only within ventral white matter (VMW) after severe (0.9 mm) spinal cord injury (SCI; L,M). Corresponding Tr maps (E–H) demonstrate generalized diffusion restriction (arrowhead—darker regions) in dorsal column and VWM, suggesting that decreased  $\lambda_{\perp}$  may result in part from ischemia. Representative luxol fast blue (LFB)-stained transverse sections of each injury group are shown in I. Reduced LFB staining in 0.9 mm injured spinal cords was investigated further with myelin basic protein immunostaining in DC (J) and VWM (K). No evidence for hyperacute demyelination is seen. (Inset J) demonstrates intact myelin rings surrounding injured SMI38-immunopositive axons within the epicenter. Error bar = 20  $\mu\text{m}$  (20 $\times$ ), 40  $\mu\text{m}$  (40 $\times$  inset). \* $p < 0.05$ . (Color image can be found online at [www.liebertpub.com/jon](http://www.liebertpub.com/jon))

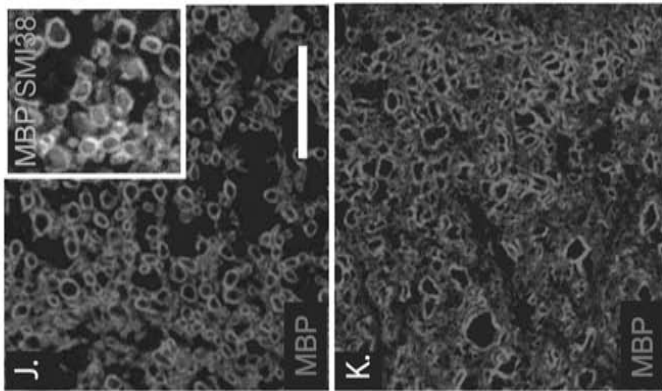
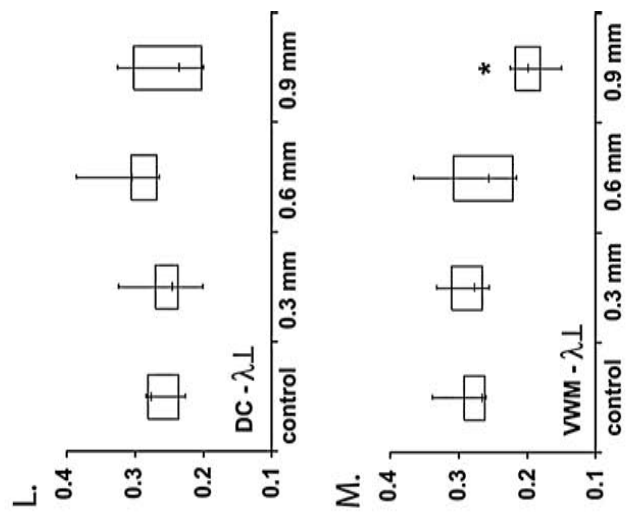
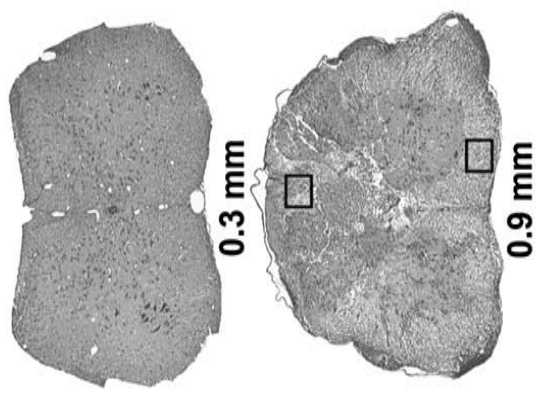
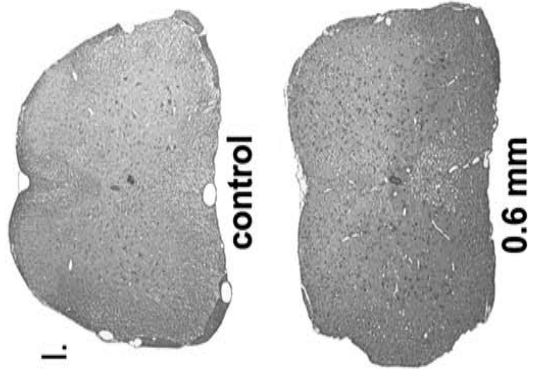
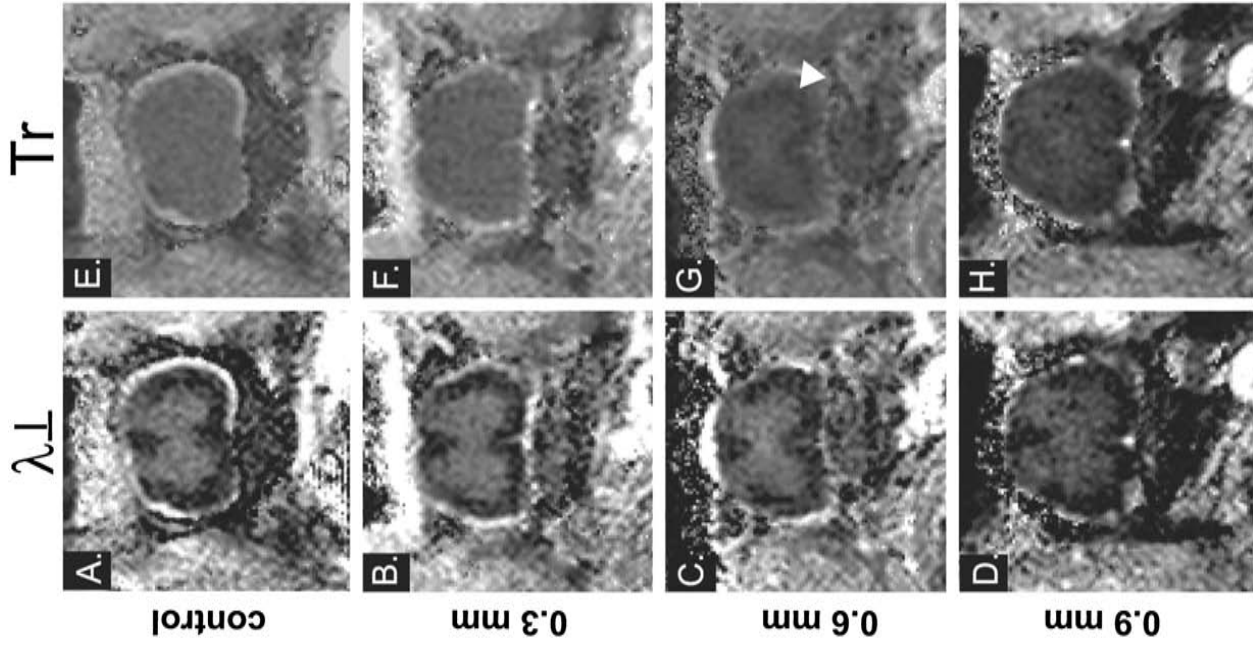


FIG. 4.

tological correlation. Regional white matter injury severity between DC and VWM varied with increasing cord displacement in a pattern consistent with spinal cord viscoelastic properties (Blight and Decrescito, 1986; Blight, 1988). DTI-detected axonal injury in the present studies may result from the ischemia in the distribution of the anterior spinal artery contributing to hyperacute SCI pathology.

The initial hours following human and experimental SCI represent an important and largely understudied gap in basic science knowledge that results in part from a lack of noninvasive measures of spinal cord pathophysiology. Currently, MRI provides the best means to study human SCI because current invasive basic science methods are impractical in the clinical arena. DTI provides unique, and quantitative measurements that have recently shed light on the physiology of rodent spinal cord (Gullapalli et al., 2006). Judicious applications of axial and radial diffusivities in CNS white matter have recently gained increasing attention (Gullapalli et al., 2006; Hasan and Narayana, 2006) because these measures correlate with the underlying pathology (Song et al., 2003; Kim et al., 2006). This approach offers a potential translation for important experimental findings derived from animal models to clinical settings. Present studies were undertaken to determine if DTI-derived axial and radial diffusivities provide useful diagnostic information in the clinically relevant hyperacute phase after experimental SCI.

RA maps provided excellent gray-white matter contrast in normal animals and within the epicenter following all SCI grades acutely, consistent with previous reports (Kim et al., 2006). Histological stains such as silver and LFB performed in this study demonstrate visible boundaries between gray and white matter. Historically, MR demarcation between gray and white matter is limited on standard T2W images because edema obscures these boundaries making identification and analysis of functionally important white matter tracts impossible, especially in more severely injured central regions. This issue is of particular importance as functional deficits following both experimental and human SCI result from damage to myelinated long tracts in the white matter. Thus, tracing of gray-white boundaries in hyperacute SCI on RA maps is beneficial for reducing quantification errors. Despite superior gray-white matter contrast, quantitative RA measurements identified only the presence or absence of moderate-to-severe SCI without any significant distinction between the two injury grades with respect to white matter.

$\lambda_{\parallel}$  provided a sensitive measure of primary axonal injury demonstrating clear quantitative differences between mild, moderate, and severe SCI grades. Present studies demonstrate a rapid decrease in white matter  $\lambda_{\parallel}$  follow-

ing hyperacute SCI corresponding to axonal injury as evidenced by silver and immunohistochemical staining (Figs. 1 and 2). Axonal injury appeared to extend outward from the central canal in a radial pattern that involved progressively more white matter with each increase in injury grade. This pattern is well-documented following standardized impactor injuries and ultimately leads to functional deficits proportional to the degree of damaged white matter (Ma et al., 2001).

The mechanisms of decreased white matter  $\lambda_{\parallel}$  following hyperacute axonal injury are likely multifactorial. Intra- and extracellular contributions to diffusion measurements after injury have not been resolved *in vivo*. Given the short time period following SCI in the present study, primary mechanical mechanisms should first be considered. Spinal cord contusion injuries result in rapid stretch of compact bundles of axons within the white matter. Depending on the velocity of the impactor tip and degree of tissue displacement, axons experience a range of tensile forces that lead to stretch or disruption as spinal cord tissue extrudes longitudinally from the center. Peak forces occur in ventral white matter tracts and increase exponentially from the dura centrally into the gray matter where disruption of spinal cord microvasculature results in variable degrees of intraparenchymal hemorrhage and edema (Blight and Decrescito, 1986; Blight, 1988; Bilgen et al., 2000). This accounts for the predominantly central pattern of necrosis and tissue loss documented extensively in the literature. At points of axonal disruption, offset of severed axonal remnants and disorganization of white matter tracts within the lesion epicenter would be expected to present microscopic barriers to diffusion, especially along the longitudinal axis ( $\lambda_{\parallel}$ ). Moreover,  $\lambda_{\parallel}$  varied regionally as predicted by viscoelastic properties of spinal cord with increasing displacement. Following mild (0.3 mm) displacement,  $\lambda_{\parallel}$  measurements suggested damage primarily to DC compared to VWM (Fig. 3). Severe displacement (0.9 mm) resulted in significantly worse injury in the VWM, consistent with reports of more pronounced axonal damage in ventral white matter following dorsal contusive injuries (Blight and Decrescito, 1986).

Observed changes in  $\lambda_{\parallel}$  likely arise in large part from the intracellular compartment also. Immediately after traumatic injury, axons enter a dynamic state of cytoskeletal reorganization and degradation. Initially, marked decreases in the distance between neurofilaments result in cytoskeletal collapse and compaction (Gallyas et al., 2002). Mitochondria swell and  $\text{Ca}^{2+}$  influx activates the neutral protease, calpain, leading to neurofilament and microtubule degradation (Maxwell, 1996; Banik et al., 1997). The ensuing breakdown in fast axonal transport causes accumulation of membranous or-

ganelles in the paranodal regions (Maxwell, 1996). The summation of these hindrances may account for decreased  $\lambda_{\parallel}$  in part.

Radial diffusion was significantly altered only in VWM and only in animals that sustained severe (0.9 mm) injuries. We have previously reported elevations in  $\lambda_{\perp}$  associated with demyelination (Song et al., 2003). It is our hypothesis that axonal damage without (or prior to) demyelination will result in a decrease in both  $\lambda_{\parallel}$  and  $\lambda_{\perp}$ . We proposed that axonal damage in the absence of demyelination will result in a readily detectable decrease of  $\lambda_{\parallel}$  (Song et al., 2003). However, the degree of decrease in  $\lambda_{\perp}$  is expected to be relatively much smaller than that in  $\lambda_{\parallel}$  and is less likely to be detectable experimentally since  $\lambda_{\perp}$  is 10–30% of  $\lambda_{\parallel}$  in magnitude. The reduction in  $\lambda_{\perp}$  observed in the present study did not contradict our previous prediction of decreased  $\lambda_{\perp}$  resulting from acute axonal injury. As previously predicted, the decreased  $\lambda_{\perp}$  tended to occur in the most severely injured (0.9 mm) regions of VWM exhibiting changes of cytotoxic edema and necrosis (Figs. 2 and 4). Both decreased  $\lambda_{\parallel}$  and  $\lambda_{\perp}$  greatly impaired the ability of RA to detect white matter injury in this report (Fig. 2L,M), strongly supporting our proposed use of  $\lambda_{\parallel}$  and  $\lambda_{\perp}$  for white matter injury assessment.

Post-traumatic ischemia may also contribute to  $\lambda_{\parallel}$ ,  $\lambda_{\perp}$ , and Tr reductions in regions exhibiting axonal injury after hyperacute SCI (Sotak, 2002; Bilgen et al., 2005). ADC reductions measured with standard clinical diffusion-weighted imaging (DWI) are characteristic of ischemia following hyperacute stroke in the brain (Sotak, 2002). Decreased ADC measurements within the spinal cord after nontraumatic ischemic injuries have also been reported recently in a small series of patients (Thurnher and Bammer, 2006). Ischemia has been implicated as the precipitating factor for glutamate release and excitotoxic secondary injury following acute SCI (Tator and Fehlings, 1991). DTI measurements presented currently may offer an advantage in the case of traumatic SCI because the integrity of functionally significant white matter tracts can also be evaluated.

In summary, present studies demonstrate that contusive SCI produces marked white matter  $\lambda_{\parallel}$  reductions that accurately predict the degree of injury severity in mice during the hyperacute phase. We have previously demonstrated that decreased  $\lambda_{\parallel}$  and increased  $\lambda_{\perp}$  are sensitive biomarkers for axonal and myelin pathology, respectively, in the subacute and chronic phases of SCI and in demyelinating disease (Kim et al., 2006; Kim et al., submitted for publication). Importantly, present studies demonstrate that  $\lambda_{\parallel}$  is also a sensitive measure of primary axonal injury in the hyperacute phase. Implications for future SCI research include the ability to obtain serial

noninvasive quantitative measurements of evolving white matter injury and to provide endpoints for monitoring experimental therapy in genetically altered strains of mice. Clinical translation of the present experiment presents many challenges associated with reduced magnetic field strengths and physical limitations of acutely injured patients. Careful correlation with clinical outcome measurements such as the American Spinal Injury Association (ASIA) impairment scale must be undertaken before DTI can be utilized as a routine diagnostic tool in the emergency setting. However, our hope is that DTI can be used to obtain much needed clinical information for the care of SCI patients and for responsible monitoring of experimental therapy trials in the future.

## ACKNOWLEDGMENTS

This study was supported in part by the National Multiple Sclerosis Society (CA 1012), NIH R01-NS047592, R01-AG10299, R01-DK19645, JDRF 1-2005-1085, University of Missouri Spinal Cord Injuries Research Program, and the Washington University Small Animal Imaging Resource (NIH R24-CA83060).

## REFERENCES

- BANIK, N.L., MATZELLE, D.C., GANTT-WILFORD, G., OSBORNE, A., and HOGAN, E.L. (1997). Increased calpain content and progressive degradation of neurofilament protein in spinal cord injury. *Brain Res.* **752**, 301–306.
- BASSER, P.J., and JONES, D.K. (2002). Diffusion-tensor MRI: theory, experimental design and data analysis—a technical review. *NMR Biomed.* **15**, 456–467.
- BILGEN, M., ABBE, R., LIU, S.J., and NARAYANA, P.A. (2000). Spatial and temporal evolution of hemorrhage in the hyperacute phase of experimental spinal cord injury: *in vivo* magnetic resonance imaging. *Magn. Reson. Med.* **43**, 594–600.
- BILGEN, M., AL-HAFEZ, B., BERMAN, N.E., and FESTOFF, B.W. (2005). Magnetic resonance imaging of mouse spinal cord. *Magn. Reson. Med.* **54**, 1226–1231.
- BLIGHT, A. (1988). Mechanical factors in experimental spinal cord injury. *J. Am. Paraplegia. Soc.* **11**, 26–34.
- BLIGHT, A.R., and DECRESCITO, V. (1986). Morphometric analysis of experimental spinal cord injury in the cat: the relation of injury intensity to survival of myelinated axons. *Neuroscience* **19**, 321–341.
- BOLDIN, C., RAITH, J., FANKHAUSER, F., HAUNSCHMID, C., SCHWANTZER, G., and SCHWEIGHOFER, F. (2006). Predicting neurologic recovery in cervical spinal

- cord injury with postoperative MR imaging. *Spine* **31**, 554–559.
- BONNY, J.M., GAVIRIA, M., DONNAT, J.P., JEAN, B., PRIVAT, A., and RENOU, J.P. (2004). Nuclear magnetic resonance microimaging of mouse spinal cord *in vivo*. *Neurobiol. Dis.* **15**, 474–482.
- DEO, A.A., GRILL, R.J., HASAN, K.M., and NARAYANA, P.A. (2006). *In vivo* serial diffusion tensor imaging of experimental spinal cord injury. *J. Neurosci. Res.* **83**, 801–810.
- EDELSTEIN, W.A., BOTTOMLEY, P.A., and PFEIFER, L.M. (1984). A signal-to-noise calibration procedure for NMR imaging systems. *Med. Phys.* **11**, 180–185.
- GALLYAS, F., FARKAS, O., and MAZLO, M. (2002). Traumatic compaction of the axonal cytoskeleton induces argyrophilia: histological and theoretical importance. *Acta Neuropathol. (Berl.)* **103**, 36–42.
- GARBOW, J.R., DUGAS, J., SONG, S.-K., and CONRADI, M. (2004). A simple, robust hardware device for passive or active respiratory gating in MRI and MRS experiments. *Concepts Magn. Reson. B* **21B**, 40–48.
- GULLAPALLI, J., KREJZA, J., and SCHWARTZ, E.D. (2006). *In vivo* DTI evaluation of white matter tracts in rat spinal cord. *J. Magn. Reson. Imaging* **24**, 231–234.
- HASAN, K.M., and NARAYANA, P.A. (2006). Retrospective measurement of the diffusion tensor eigenvalues from diffusion anisotropy and mean diffusivity in DTI. *Magn. Reson. Med.* **56**, 130–137.
- KIM, J.H., BUDDE, M.D., LIANG, H.F., et al. (2006). Detecting axon damage in spinal cord from a mouse model of multiple sclerosis. *Neurobiol. Dis.* **21**, 626–632.
- LE BIHAN, D., MANGIN, J.F., POUPON, C., et al. (2001). Diffusion tensor imaging: concepts and applications. *J. Magn. Reson. Imaging* **13**, 534–546.
- MA, M., BASSO, D.M., WALTERS, P., STOKES, B.T., and JAKEMAN, L.B. (2001). Behavioral and histological outcomes following graded spinal cord contusion injury in the C57Bl/6 mouse. *Exp. Neurol.* **169**, 239–254.
- MADI, S., HASAN, K.M., and NARAYANA, P.A. (2005). Diffusion tensor imaging of *in vivo* and excised rat spinal cord at 7T with a icosahedral encoding scheme. *Magn. Reson. Med.* **53**, 118–125.
- MAXWELL, W.L. (1996). Histopathological changes at central nodes of Ranvier after stretch-injury. *Microsc. Res. Tech.* **34**, 522–535.
- SCHWARTZ, E.D., and HACKNEY, D.B. (2003). Diffusion-weighted MRI and the evaluation of spinal cord axonal integrity following injury and treatment. *Exp. Neurol.* **184**, 570–589.
- SHEPARD, M.J., and BRACKEN, M.B. (1999). Magnetic resonance imaging and neurological recovery in acute spinal cord injury: observations from the National Acute Spinal Cord Injury Study 3. *Spinal Cord* **37**, 833–837.
- SONG, S.K., SUN, S.W., JU, W.K., LIN, S.J., CROSS, A.H., and NEUFELD, A.H. (2003). Diffusion tensor imaging detects and differentiates axon and myelin degeneration in mouse optic nerve after retinal ischemia. *Neuroimage* **20**, 1714–1722.
- SOTAK, C.H. (2002). The role of diffusion tensor imaging in the evaluation of ischemic brain injury—a review. *NMR Biomed.* **15**, 561–569.
- STEJSKAL, E.O., and TANNER, J.E. (1965). Spin echoes in the presence of a time-dependent field gradient. *J. Chem. Physics* **42**, 288–292.
- SUN, S.W., SONG, S.K., HONG, C.Y., CHU, W.C., and CHANG, C. (2003). Directional correlation characterization and classification of white matter tracts. *Magn. Reson. Med.* **49**, 271–275.
- SUNDGREN, P.C., DONG, Q., GOMEZ-HASSAN, D., MUKHERJI, S.K., MALY, P., and WELSH, R. (2004). Diffusion tensor imaging of the brain: review of clinical applications. *Neuroradiology* **46**, 339–350.
- TATOR, C.H., and FEHLINGS, M.G. (1991). Review of the secondary injury theory of acute spinal cord trauma with emphasis on vascular mechanisms. *J. Neurosurg.* **75**, 15–26.
- THURNHER, M.M., and BAMMER, R. (2006). Diffusion-weighted MR imaging (DWI) in spinal cord ischemia. *Neuroradiology* **48**, 795–801.
- ZHANG, S.X., UNDERWOOD, M., LANDFIELD, A., HUANG, F.F., GISON, S., and GEDDES, J.W. (2000). Cytoskeletal disruption following contusion injury to the rat spinal cord. *J. Neuropathol. Exp. Neurol.* **59**, 287–296.

Address reprint requests to:  
 Sheng-Kwei Victor Song, Ph.D.  
 Biomedical MR Laboratory  
 Campus Box 8227  
 Washington University School of Medicine  
 Room 2313, 4525 Scott Avenue  
 St. Louis, MO 63110

E-mail: ssong@wustl.edu